Papers submitted to the Conference "Applications of Physics in Mechanical and Material Engineering"

The Influence of $\mathcal{PT}$ Symmetry Breaking on the Chaotic Properties of the Coupled Magnetic Pendulums System

A. Szewczyk[a], W. Leoński[a] and R. Szczęśniak[b,c]

[a] *Quantum Optics and Engineering Division, Faculty of Physics and Astronomy, University of Zielona Góra, Prof. Z. Szafrana 4a, 65-516 Zielona Góra, Poland*
[b] *Division of Physics, Częstochowa University of Technology, Armii Krajowej Ave. 19, 42-200 Częstochowa, Poland*
[c] *Division of Theoretical Physics, Jan Długosz University in Częstochowa, Armii Krajowej Ave. 13/15, 42-200 Częstochowa, Poland*

Doi: 10.12693/APhysPolA.142.52 *e-mail: aszewczyk@yahoo.com

The influence of the $\mathcal{PT}$-symmetry breaking on the chaotic properties of the coupled magnetic pendulums is investigated. The $\mathcal{PT}$-symmetric system is described by the classical approach using coupled second-order nonlinear differential equations. Using the damping coefficient A as the control parameter for the $\mathcal{PT}$-symmetry and evaluating the two-dimensional basin plot of the pendulum's motion, the fractal of measure for unbroken $\mathcal{PT}$-symmetry is calculated to be $D_f \simeq 2$ and changes to $D_f \simeq 1.25$ for broken symmetry.

topics: parity–time ($\mathcal{PT}$) symmetry

1. Introduction

Deterministic chaos is a simulation of randomness and unpredictable behavior of a nonlinear dynamic system. Turing [1], Poincare [2], and Birkhoff [3] were the first to observe that some mathematical models show a sensitive dependence on initial conditions. But it was James Jorke [4] who defined chaos and fully described its properties. Later, Edward Lorenz [5] made a major contribution, expanding the understanding of deterministic chaos. This theory has evolved and branched out into new research fields such as weather analysis, ecology dynamics [6], self-assembly processes [7], edge of chaos theory [6], and complex dynamical systems.

To simulate deterministic chaos, one could experiment with, for example, a magnetic pendulum [8] or derive its mathematical model [9–11] using classical mechanics and run numerical simulations. Tran's work [8] confirmed the deterministic properties of the system by matching the experimental measurements with the theory using Poincare sections. Christian [9] has demonstrated that chaos can be visualized with pendulum's attractors called basins. Kwuimy's analysis [10] has indicated the influence of the damping control parameter on the chaotic motion of the pendulum. Another way of investigating chaos is by the mechanical coupling of two pendulums with a spring. Dudkowski [12] calculated that the stability of the coupled pendulum basin depends on the values of the system's control parameters.

Some dynamic systems can also exhibit a particular form of symmetry. Parity–time ($\mathcal{PT}$) symmetry is a property of a system that has a Hamiltonian and is not necessarily energy conserved. Bender [13–15] introduced this concept using classical physics. Further studies of $\mathcal{PT}$-symmetry and oscillators have been done by Tsoy [16]. Tsoy determined that for the oscillator to reach a stationary state, its energy gain and energy loss must be well balanced. Such property has many useful applications in other fields of physics. Further studies have been done in classical mechanics [16], energy harvesting [17, 18], electronics [19], and optics [20].

The objective of this paper is to combine the $\mathcal{PT}$-symmetry property with complex pendulum dynamics to determine the relationship between $\mathcal{PT}$-symmetry and chaos. To answer this question, a simple classical physics model [16, 21], such as a spring-coupled magnetic pendulum, was made to numerically calculate the properties and conditions for broken/unbroken $\mathcal{PT}$-symmetry. This model is new as it inherits and combines all the features of previous studies [9, 16].

2. Model

A spring-coupled magnetic pendulum is a device that consists of two pendulums connected to each other by a spring. Both pendulums are suspended to move freely in the x–y plane. The bob's motion is also influenced by any number of magnets positioned on the x–y plane at some distance from the stationary position of the bob. The formulae used to describe the magnets distribution in the x–y plane are $x_i = R\cos(2\pi i/n)$ and $y_i = R\sin(2\pi i/n)$, where i is a magnet count, R is the radius of a circle, and n is the maximum number of magnets. In the model, the distribution of the position of the magnet is placed on the circumference of a circle. The centroid of distribution coincides with the pendulum suspension position in the x–y plane. For each pendulum, the position and distribution of the magnets in the x–y plane are made in such a way that the magnets' distances are equal.

Some assumptions are made to simplify this model and to make it easier to derive the spring-coupled second-order differential equations of the magnetic pendulums. It is assumed that the pendulum experiences mechanical friction, and the aerodynamic drag on the bob is considered negligible. The spacing between the magnets in the x–y plane is much smaller than the pendulum's length. The height of the bob from the x–y plane and their x–y coordinates values are small compared to the length of the pendulum.

The equations of motion for a spring coupled magnetic pendulum have the form of

$$\ddot{x}_a + A\dot{x}_a + Bx_a + \sum_{i=1}^{n}\left[\frac{C(x_a - x_{ia})}{\left((x_{a,i}-x_a)^2 + (y_{a,i}-y_a)^2 + h^2\right)^{\frac{3}{2}}}\right] + D(x_a - x_b)\left[1 - \frac{\sqrt{(x_{0b}-x_{0a})^2 + (y_{0b}-y_{0a})^2}}{\sqrt{(x_b-x_a)^2 + (y_b-y_a)^2}}\right] = 0, \tag{1}$$

$$\ddot{y}_a + A\dot{y}_a + By_a + \sum_{i=1}^{n}\left[\frac{C(y_a - y_{ia})}{\left((x_{a,i}-x_a)^2 + (y_{a,i}-y_a)^2 + h^2\right)^{\frac{3}{2}}}\right] + D(y_a - y_b)\left[1 - \frac{\sqrt{(x_{0b}-x_{0a})^2 + (y_{0b}-y_{0a})^2}}{\sqrt{(x_b-x_a)^2 + (y_b-y_a)^2}}\right] = 0, \tag{2}$$

$$\ddot{x}_b - A\dot{x}_b + Bx_b + \sum_{i=1}^{n}\left[\frac{C(x_b - x_{ib})}{\left((x_{b,i}-x_b)^2 + (y_{b,i}-y_b)^2 + h^2\right)^{\frac{3}{2}}}\right] + D(x_b - x_a)\left[1 - \frac{\sqrt{(x_{0b}-x_{0a})^2 + (y_{0b}-y_{0a})^2}}{\sqrt{(x_b-x_a)^2 + (y_b-y_a)^2}}\right] = 0, \tag{3}$$

$$\ddot{y}_b - A\dot{y}_b + By_b + \sum_{i=1}^{n}\left[\frac{C(y_b - y_{ib})}{\left((x_{b,i}-x_b)^2 + (y_{b,i}-y_b)^2 + h^2\right)^{\frac{3}{2}}}\right] + D(y_b - y_a)\left[1 - \frac{\sqrt{(x_{0b}-x_{0a})^2 + (y_{0b}-y_{0a})^2}}{\sqrt{(x_b-x_a)^2 + (y_b-y_a)^2}}\right] = 0. \tag{4}$$

The definitions of the coefficients are $A = f/m$, $B = g/L$, $C = k/m$ and $D = k_s$. The symbols f and m are defined as the drag constant and the mass of the bob, respectively. The g-factor is the gravity acceleration and L — the pendulum's length. The constant k is the magnetic coefficient and k_s is the spring coefficient. The position of i-th magnet for the pendulum a and b is $(x_{a,i}, y_{a,i})$ and $(x_{b,i}, y_{b,i})$, respectively; h is defined as the height between the bob's z position and the x–y plane at rest.

The initial conditions for pendulums are

$$\begin{aligned} &x_a(0) = x_{0a} \quad y_a(0) = y_{0a}, \\ &\dot{x}_a(0) = 0, \quad \dot{y}_a(0) = 0, \\ &x_b(0) = x_{0b}, \quad y_b(0) = y_{0b}, \\ &\dot{x}_b(0) = 0, \quad \dot{y}_b(0) = 0. \end{aligned} \tag{5}$$

3. Results

A direct analytical approach for this model is very challenging, if not impossible. The first and obvious approach is to linearize the nonlinear components (magnetic and spring force) in (1)–(4). This can be done with the Taylor series expansion method, keeping only the constant and the first term. One can then use the modified linearized system to find the $\mathcal{PT}$-symmetric conditions that are only dependent on the values of A, B, C, and D. Another common method is to use the Jacobian matrix method, which linearizes the nonlinear system at critical points. However, quick calculations showed that both methods are incorrect because they yield

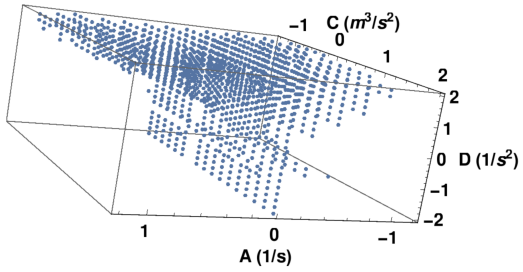

Fig. 1. A 3D plot of values for input parameters A, C, and D.

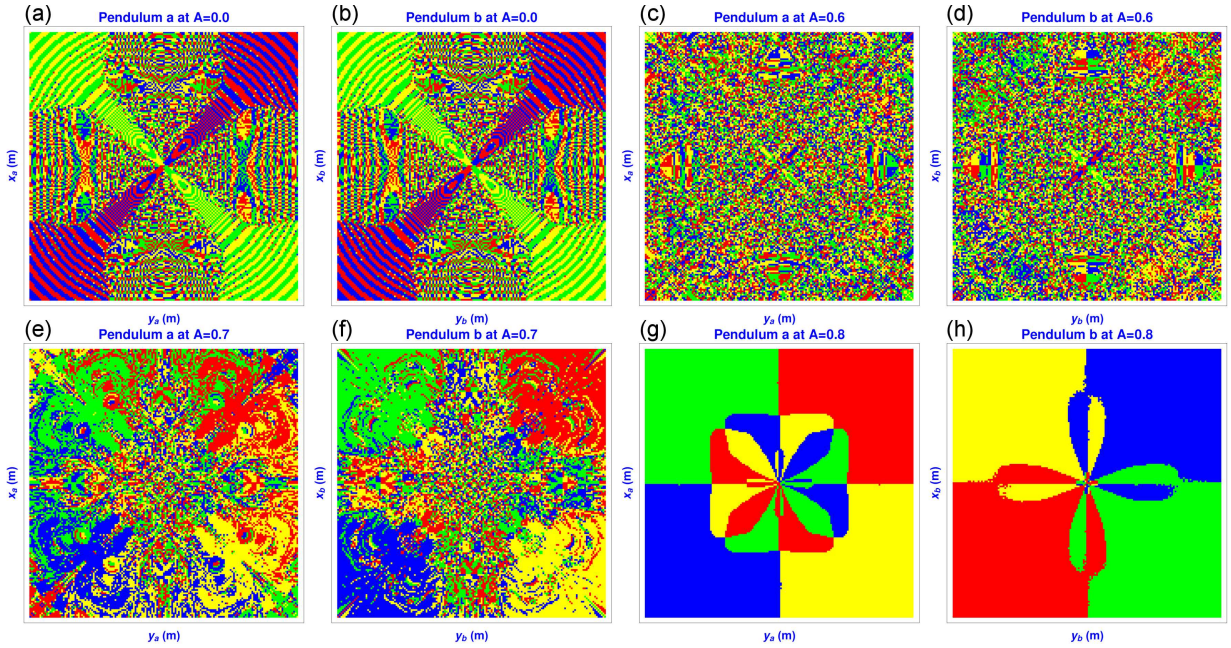

Fig. 2. Basins of pendulum a and b for A values of 0.0, 0.6, 0.7, and 0.8. Note: $B = 0.98$, $C = 1.6$, and $D = 1.0$.

inconsistent results. Therefore, the Monte Carlo approach is being considered. The new numerical algorithm relies on the Fourier transform and convolution calculations. The following, accordingly listed conditions apply in the numeric

1. the real and imaginary part of the convolution taken over the product composed of the x-axis (y-axis) amplitudes of the pendulums a and b should be less than one,
2. the product of the Fourier transform for each pendulum's amplitude in the x-axis (y-axis) and the periodogram spectrum amplitude must be all negative,
3. the variance of the Fourier transform in the x-axis (y-axis) amplitude should be less than one.

To evaluate the performance of this algorithm, a Bender analytical result [15] is used for comparison. The numerical results are in close agreement with the analytical calculation for the Bender's system.

When searching for $\mathcal{PT}$-symmetric unbroken conditions using the Monte Carlo method, a range of values for A, C, and D are collected. Figure 1 summarizes the calculated values for $B = 0.98$ that satisfy the numerically defined symmetry conditions.

Using the obtained data ($A = 0.2$, $C = 1.6$, and $D = 1$), a plot of the position of the a and b pendulums (both x and y) is made to verify the numerical method. A constant amplitude for both pendulums in the x-axis for the entire time spectrum suggests that, according to Bender's theory, the input and output of energies are in the equilibrium phase and there is no net gain or loss in energy. Therefore, the

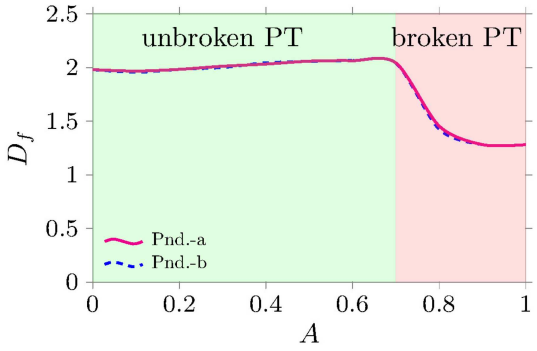

Fig. 3. Fractal measure D_f for range of A.

coupled system is $\mathcal{PT}$-symmetric on the x-axis. On other hand, the y-axis shows a small gain in amplitude for both pendulums, even when their initial y-axis values were set to zero. It could be due to numerical noise or the transfer of energy from one axis to another. The results demonstrate the effectiveness of $\mathcal{PT}$-algorithm search in screening out the values that create an unbroken symmetry system.

Figure 2 shows the basins of attractors for pendulums a and b. The expectation for unbroken symmetry is that the basin for each pendulum should be almost identical due to the near-exact amplitude oscillations, and the numerical plots confirm that. Figure 2e–h ($A = 0.7$ and $A = 0.8$) shows the significant difference in the basin plot of both pendulums. This is due to the broken $\mathcal{PT}$-symmetry, therefore there is an energy gain of the system that can be observed in the amplitude plots.

Figure 3 illustrates the relationship between the fractal dimension (D_f) of basins and the $\mathcal{PT}$ symmetry, where D_f is the Minkowski–Bouligand dimension. It is commonly referred to as the box-counting dimension and is defined as

$$D_f = \lim_{\varepsilon \to 0} \frac{\ln\left(N(\varepsilon)\right)}{\ln\left(\frac{1}{\varepsilon}\right)}. \tag{6}$$

The symbol $N(\varepsilon)$ is the number of boxes and ε is the side length required to cover the pixels of an image. The obtained D_f values are nearly identical in the spectrum range of A. During the unbroken $\mathcal{PT}$-symmetry condition phase, the fractal dimension remains near the value of 2. Then D_f becomes $\simeq 1.25$ for the broken $\mathcal{PT}$-symmetry condition.

4. Conclusion

The numerical analysis of the spring coupled magnetic pendulum system shows that it is possible to determine the $\mathcal{PT}$-symmetry of a strongly nonlinear coupled differential system without relying on analytical methods. Using Bender's simple coupled model [15] as a reference, a numerical approach can be deduced to verify a system of greater complexity. The conditions outlined in the paper are sufficient to numerically determine whether the system is $\mathcal{PT}$-symmetric or not. Using this method, the values of input parameters A, C, and D can be determined to make the coupled system $\mathcal{PT}$-symmetric. The numerical analysis demonstrated that the Minkowski–Bouligand dimension D_f for unbroken $\mathcal{PT}$-symmetry is approximately 2 and changes to ~ 1.25 for broken symmetry.

References

[1] A. Turing, *Philos. Trans. R. Soc. Lond. B* **641**, 3772 (1952).

[2] H. Poincare, *Les Methodes Nouvelles de la Mécanique Céleste*, Grauthier-Viltars, 1892.

[3] G.D. Birkoff, Dynamical Systems, Colloquium Publications, 1927.

[4] Tien-Yien Li, J.A. Yorke, *Am. Math. Monthly* **82**, 985 (1975).

[5] E. Lorenz, *J. Atmos. Sci.* **20**, 130141 (1963).

[6] R. K. Upadhyay, *Appl. Math. Comput.* **381**, 455464 (2009).

[7] E. Wetterskog, M. Agthe, A. Mayence, J. Grins, Dong Wang, S. Rana, A. Ahniyaz, G. Salazar-Alvarez, L. Bergström, *Sci. Technol. Adv. Mater.* **214**, 055010 (2014).

[8] V. Tran, E. Brost, M. Johnston, J. Jalkio, *Chaos* **23**, 033103 (2013).

[9] J. M. Christian, H.A.J. Middleton-Spencer, *Math. Today* **56**, 70 (2020).

[10] C.K. Kwuimy, M. Belhaq, C. Nataraj, *Math. Probl. Eng.* **2012**, 18 (2012).

[11] S. D'Alessio, *Phys. Educ.* **50**, 3 (2020).

[12] D. Dudkowski, K. Czołczyński, T. Kapitaniak, *Chaos* **29**, 10 (2019).

[13] C.M. Bender, *PT Symmetry In Quantum and Classical Physics*, World Scientific, 2019.

[14] C.M. Bender, *Rep. Prog. Phys.* **70**, 947 (2007).

[15] C.M. Bender, B.K. Berntson, D. Parker, E. Samuel, *Am. J. Phys.* **81**, 173 (2013).

[16] E.N. Tsoy, *Phys. Lett. A* **210**, 462 (2017).

[17] L.J. Fernandez-Alcazar, R. Kononchuk, T. Kottos, *Commun. Phys.* **4**, 9 (2021).

[18] B. Ambrożkiewicz, G. Litak, P. Wolszczak, *Appl. Sci.* **10**, 14 (2020).

[19] J. Schindler, Z. Lin, J.M. Lee, H. Ramezani, F.M. Ellis, T. Kottos, *J. Phys. A: Math. Theor.* **45**, 17 (2012).

[20] C.E. Rüter, K.G. Makris, R. El-Ganainy, D.N. Christodoulides, M. Segev, D. Kip, *Nat. Phys.* **6**, 192 (2010).

[21] A.E. Motter, M. Gruiz, G. Károlyi, T. Tél, *Phys. Rev. Lett.* **111**, 194101 (2013).